Solidification Reaction Sequence of Co-Rich Nb-Al-Co Alloys

L.M. FEITOSA, N. D'SOUZA, G.D. WEST, and H.B. DONG

The freezing reaction sequence of Co-rich Nb-Al-Co ternary alloys with emphasis on the formation of Laves and Heusler phases has been examined. For Co-rich alloys, the solidification reaction sequence is observed as primary freezing of α-Co and CoAl phases, subsequent [Co + C36] and [CoAl + C36] eutectics, and the final ternary eutectic reaction [L → α-Co + C36 + CoAl]. The compositions of solidified α-Co and C36 phases agree with the corresponding vertices of the tie-triangle at the solidus temperatures. When the Nb concentration is over 20 at. pct in Co-rich alloys, the quasi-peritectic reaction [L + Co_2AlNb → C36 + CoAl] does not occur as equilibrium prediction. The formation of C36 and CoAl phases occurs through solid precipitation and must be distinguished from a solidification reaction.

I. INTRODUCTION

THE natural choice of materials for high-temperature applications, such as in turbines in aero-engine applications, is Ni-base superalloys owing to their excellent combination of strength, ductility, and high-temperature oxidation properties.[1,2] However, with increasing demands on efficiency and step increase in turbine entry temperatures, there has been a keen interest in the development of alternative alloy systems.[3] One alternative that has been explored refers to the RM-Al-X system, where RM = Ta, Nb and X = Pd, Fe, Ti. For instance, it has been demonstrated that in the Pd-Al-Nb system, the ordered B2 precipitates present in the disordered A2 matrix constitute the strengthening phase.[4] This principle, in fact, is similar to that in the Ni-base alloys, where the ordered γ′ (L1$_2$) precipitate in the disordered A1 fcc matrix provides the high-temperature strength, while the matrix is ductile.[5–7] Also, the beneficial role of Al is to impart oxidation resistance through the formation of a continuous layer of Al_2O_3. Alternatively, the intermetallic Laves phase in iron-aluminide alloys has also been identified as a promising candidate for structural applications.[8–10] Laves phases show outstanding strength at elevated temperatures above 1273 K (1000 °C) but are brittle at room temperature due to their structures.[9,11] It has been shown that Ta is an important alloying addition to Fe-Al, as it can form the ternary Laves phase with the hexagonal C14 structure.[9] Recent investigations indicate that, in addition to the formation of the $(Fe,Al)_2Ta$ Laves phase, when Ta is added to Fe_3Al, there is the unexpected formation of the Heusler-type phase.[12] It is not surprising, therefore, that the Fe-Al-Ta system has been studied with an emphasis on the Laves and Heusler phases, and on the relationship existing between alloy composition, phase stability, microstructure, and mechanical properties.[13,14] Another ternary, the Co-Al-Nb alloy system, exists, in which both the ternary Laves phase and the Heusler phase, Co_2AlNb, occur.[15–17] Additionally, unlike the Fe-Al-Ta ternary, the Co-Al-Nb system is of significant interest for the fundamental understanding of the stability of different types of poly types of Laves phase. This is because all three types of Laves phase, hexagonal C14 and C36 as well as cubic C15, are stable in the binary Co-Nb system.[18,19] It is this alloy system that is the subject of investigation in the current study.

From metallographic observations of as-cast microstructures, composition analyses, and differential thermal analysis, a liquidus projection was determined in the ternary Co-Al-Nb system and the solidification path was determined for a number of compositions in the different two- and three-phase regions.[20] However, in ternary systems, there are some additional aspects that need to be considered while addressing the solidification path. During primary phase growth, unlike in binary systems, an added degree of freedom exists.[21,22] Therefore, the path traversed by the liquid composition on the liquidus surface will be contingent on microsegregation, i.e., the extent of back diffusion within the

L.M. FEITOSA and H.B. DONG are with the Department of Engineering, University of Leicester, Leicester, LE1 7RH, UK. Contact email: hd38@le.ac.uk N. D'SOUZA is with Rolls-Royce plc, Derby, DE24 8BJ, UK. G.D. WEST is with the Warwick Manufacturing Group, University of Warwick, Coventry, CV4 7AL, UK.

solid.[23] This, in turn, will not only dictate the evolution of solid fraction but, importantly in the ternary system, also determine where the liquid composition intersects the monovariant line (eutectic valley or peritectic) that marks the end of primary freezing, if all the liquid has not been consumed.[24] Two cases can arise:

(1) If there is a gradual transition in the monovariant line, from, say, a peritectic to a eutectic reaction, across the liquidus surface while proceeding to lower temperatures, then the path followed by the liquid composition will dictate the nature of the three-phase reaction that will result, *i.e.*, peritectic or eutectic depending on the intersection.[25–27]

(2) If an invariant point exists, then two of the three monovariant lines emanating from this point will enclose the liquidus surface of the primary phase. The path traversed by the liquid composition during primary freezing will then determine which of these two monovariant lines the liquid composition will intersect at the end of primary freezing. This will then determine the resulting three-phase reaction, which might or might not preclude the subsequent invariant reaction at lower temperature. This explains the unexpected occurrence of the $(L \rightarrow A2 + \mu)$ eutectic reaction in the Ta-Al-Fe system, instead of the peritectic reaction $(L + A2 \rightarrow \sigma)$ in the Ta-rich corner, following primary freezing of A2. Also, in some cases, suppression of the Class II invariant reaction, $L + \sigma \rightarrow A2 + \mu$, might occur.[28,29] Likewise, in the Pb-Sn-Sb system during rapid cooling following nucleation and growth of primary Sb, the liquid composition approaches the Sb-Pb eutectic valley instead of the Sb-Sn eutectic valley, resulting in the $(L \rightarrow Sb + Pb)$ eutectic reaction instead of the $(L \rightarrow Sb + SbSn)$ eutectic reaction.[30]

Both (1) and (2) will then have an important role in the subsequent invariant reactions, if these do occur, and on the subsequent three-phase reactions that result, when not all the liquid has been consumed. In the case of the invariant reactions, some additional important points need to be emphasized. In a binary system for an invariant reaction with three phases (L, α, β):

(1) Eutectic—The three phases grow together and are coincident along a line, where the compositions in the phases follow the tie-line $(L \rightarrow \alpha + \beta)$. Remote from this line, primary growth of the two phases occurs as $L \rightarrow \alpha$ and $L \rightarrow \beta$, respectively.

(2) Peritectic—The three phases are coincident along a line, where the peritectic reaction occurs $(L + \alpha \rightarrow \beta)$. This is governed by diffusion in the liquid, leading to a rim of peritectic β phase formed across primary α and given by the two reactions $L \rightarrow \beta$ and $\alpha \rightarrow L$. Since diffusion in the solid is limited, the subsequent peritectic transformation is inhibited and growth of β occurs through primary freezing as $L \rightarrow \beta$.[31,32]

However, in a ternary system corresponding to an invariant reaction, four phases are involved $(L, \alpha, \beta, \gamma)$.

In this case, the coincidence of all phases will only occur at a point, though nucleation, at a point, is meaningless. Moreover, nucleation of the third solid phase will necessarily occur on one of the two existing solid phases, and growth of this third phase must involve a three-phase reaction. Therefore, it is unlikely that solidification will terminate at the invariant point. In the current study, the focus is on the invariant reactions in the Co-rich corner of the Gibbs triangle in the Co-Al-Nb ternary system and involving the Laves and Heusler phases. These will involve Class I and II reactions, and the compositions are indicated on the liquidus projection in Figure 1(a). Also included in Figure 1(b) is the isothermal section at 1473 K (1200 °C), and superimposed on this projection are the limits of solute solubility at 1073 K (800 °C).[15] The focus in this article, therefore, is twofold.

(1) α-Co, C36, CoAl phases in the Co-rich corner—S1, S2 (Table I): An analysis of primary freezing of Co and CoAl phases occurred at temperatures around 1553 K (1280 °C) and 1573 K (1300 °C), respectively, while the ternary eutectic [Co + C36 + CoAl] freezes at 1493 K (1220 °C). The emphasis will be on measurement of the solubility limits in the various phases.[15,20]

(2) C14, Co$_2$AlNb, C36, CoAl phases in the Co-rich corner—S3, S4, S5, S6 (Table I): The focus here will be on primary freezing of C14, which takes place in the temperature range of 1673 K to 1753 K (1400 °C to 1480 °C) and subsequent eutectic reaction preceding the Class II reaction, $L + Co_2AlNb \rightarrow C36 + CoAl$.[15] Specifically, given the very narrow tie-triangle at 1523 K (1250 °C)
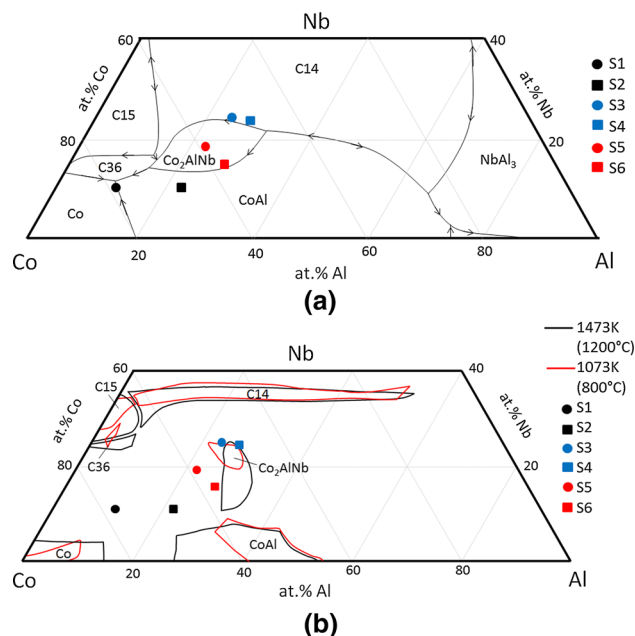

(a)

(b)

Fig. 1—(a) Liquidus projection[20] and (b) isothermal section at 1473 K (1200 °C) with superimposed limits of solute solubility at 1073 K (800 °C).[15] The compositions in this study are superimposed in the figures.

Table I. Nominal Compositions of the Alloys Studied (in At. Pct), Phases Expected Following Ref. [15], and Actual Phases Observed in the Microstructure

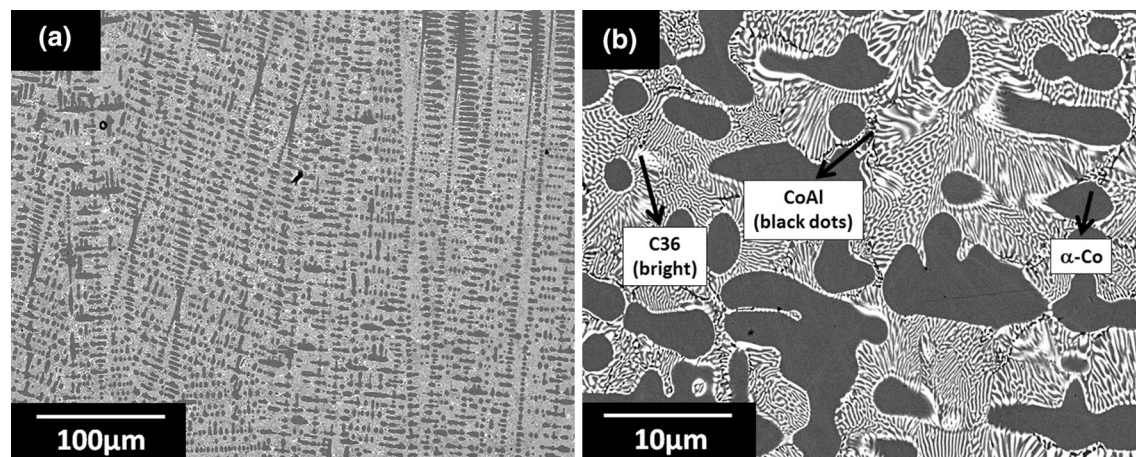| Sample	Pct Nb	Pct Co	Pct Al	Phases Expected [at 1073 K (800 °C)][15]	Phases Observed
S1	9.9	78.5	11.6	Co + C36 + CoAl	Co + C36 + CoAl
S2	10.0	68.4	21.6	Co + C36 + CoAl	Co + C36 + CoAl
S3	23.3	46.1	22.6	C14 + Co_2AlNb	C14 + Co_2AlNb
S4	24.5	49.1	26.4	C14 + Co_2AlNb	C14 + Co_2AlNb
S5	19.4	58.5	22.1	Co_2AlNb + C36 + CoAl	Co_2AlNb + C36 + CoAl
S6	15.0	58.5	26.5	Co_2AlNb + C36 + CoAl	Co_2AlNb + C36 + CoAl

Fig. 2—BEI of microstructure corresponding to alloy S1: (*a*) low magnification and (*b*) high magnification.

compared with that at 1073 K (800 °C), the possibility of a solid-state reaction leading to nucleation and growth of the CoAl phase will be considered. The implications of this on the solubility limits in the different phases will be examined.

II. EXPERIMENTAL METHODS AND MATERIALS

Samples were produced using arc melting, which involved melting of elemental powders on a cooled Cu hearth. With this method, small ingots of approximately 40 g of each alloy were cast via arc melting on a water-cooled hearth in an evacuated and argon back-filled atmosphere. Elemental metals, with purity ≥99.9 pct, were used as the feedstock and to minimize the loss of Al during the melting process, the alloys were fabricated in a two-step procedure. A binary alloy was created from the refractory and transition metals and was then melted with pure Al to create the final ingot. To increase the homogeneity of both the binary and ternary alloys, at least two remelting operations were used at each stage, in between which the ingots were physically inverted on the hearth.

All scanning electron microscopy was performed using a beam (Philips XL 30 environmental scanning electron microscope). Backscattered electron images (BSEs) were collected using a retractable solid-state backscatter detector using high (20 kV) electron beam accelerating voltages for enhanced compositional contrast. Chemical analysis was undertaken in this system at 20 kV using energy-dispersive spectroscopy. The nominal composition of the alloys studied and the expected phases according to the phase diagrams and the actual phases observed in the microstructure is presented in Table I.

Phase identification was undertaken using an Empyrean (PANalytical) X-ray diffractometer. The system used Co as the anode material and was operated at 40 kV with a tube current of 40 mA. Spectra were collected in the scan range (20 to 120 deg) corresponding to 2θ with a step size of 0.013 deg.

III. RESULTS AND DISCUSSION

A. *Class I—Ternary Eutectic Reaction*

Figure 2(a) is a low-magnification BEI corresponding to S1, where α-Co, CoAl, and C36 are the expected phases in the as-cast microstructure. The composition of α-Co primary dendrites (gray) is presented in Table II, where the uncertainty corresponds to the standard deviation arising from the multiple measurements that were made. The (α-Co + C36) eutectic morphology is lamellar, indicating cooperative growth, where the white phase is C36. The sporadic CoAl (dark) phase forms as the ternary eutectic, as observed in the high-magnification BEI in Figure 2(b). Owing to the scale of the

Phase	Pct Al	Pct Co	Pct Nb
α-Co (S1)	12.9 ± 0.05	83.1 ± 0.05	4.1 ± 0.06
CoAl (Dark Core) (S2)	32.1 ± 1.42	62.1 ± 1.23	5.8 ± 0.25
CoAl (Periphery) (S2)	27.0 ± 1.10	67.0 ± 0.76	6.0 ± 0.36
C36 (Coarse Cellular) (S2)	6.5 ± 0.17	69.9 ± 0.19	23.7 ± 0.27
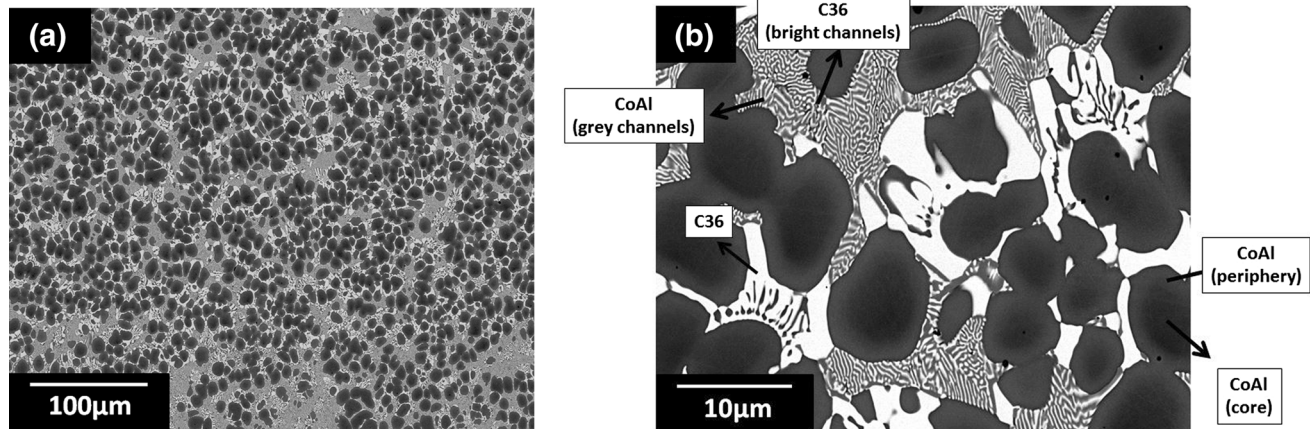
Fig. 3—BEI of microstructure corresponding to alloy S2: (*a*) low magnification and (*b*) high magnification.

microstructure and to prevent volume averaging,[33] composition measurements were restricted to within α-Co phase in S1.

Figure 3(a) is a low-magnification BEI corresponding to S2, where, in this case, the primary phase is CoAl. The higher magnification BEI in Figure 3(b) shows that distinct coring is present across primary CoAl, which is also evident in the average composition measurements in Table II. The [CoAl + C36] eutectic morphology shows a transition from lamellar to coarse cellular. The composition within the coarse cellular C36 morphology was also measured.

Further, in order to definitively confirm the presence of the ternary eutectic in S2 to justify the comparison to the tie-triangle, X-ray diffraction was carried out to identify the phases in both S1 and S2. XRD patterns for S1 and S2 are presented in Figures 4(a) and (b), respectively, from which it can be unequivocally ascertained that α-Co does occur as a ternary eutectic in S2, as in the case of S1.

It is clear that, unlike in the case of CoAl, there is negligible microsegregation within either α-Co or C36. The measured compositions are plotted in the isothermal section at 1473 K (1200 °C) in Figure 5.[15] Also, given that changes in solute solubility can occur during cooling in the solid phase, changes in solute solubility in the different phases at 1073 K (800 °C) are also superimposed in Figure 5.[15] Both the α-Co and C36 measured compositions are in good agreement with the respective vertices in the tie-triangle in the isothermal section at 1473 K (1200 °C), but this is not so in the case of CoAl. Since we are concerned with the freezing path, it is important to consider isothermal sections that are close to where freezing would terminate, since

isothermal sections constructed at lower temperatures correspond to fully heat-treated conditions where there can be appreciable changes in solute solubility. Therefore, in this case, we merely compare our measured compositions with those represented by tie-lines or tie-triangles in the relevant isothermal sections. Accordingly, for alloys S1 and S2, the isothermal section at 1473 K (1200 °C) was used, while the isothermal section at 1523 K (1250 °C) will be used for alloys S3 through S6, as these were higher melting alloys. While the Nb composition in both the dendrite core and periphery is similar to that in the isothermal section, the measured composition shows a higher Al (and lower Co) concentration in the dendrite core compared to the periphery. Further, comparison with the isothermal section at 1073 K (800 °C) shows that α-Co is supersaturated in Al. The absence of microsegregation in primary α-Co also precludes microsegregation during subsequent eutectic freezing, L → α-Co + C36. The solidus temperature for the ternary reaction is 1493 K (1220 °C).[20] Since the measured composition within primary α-Co is also in good agreement with the corresponding vertex in the tie-triangle at 1473 K (1200 °C), it can be concluded, therefore, that this composition of α-Co also corresponds to that at the onset of freezing of the ternary eutectic. In the case of CoAl being the primary phase in S2 and where appreciable microsegregation exists, the dendrite core composition is in good agreement with the vertex of the tie-triangle, while the dendrite periphery instead is supersaturated in Co (depleted in Al). The changing composition from dendrite core to periphery arises from coring (microsegregation) during solidification and arising from limited solute solubility.
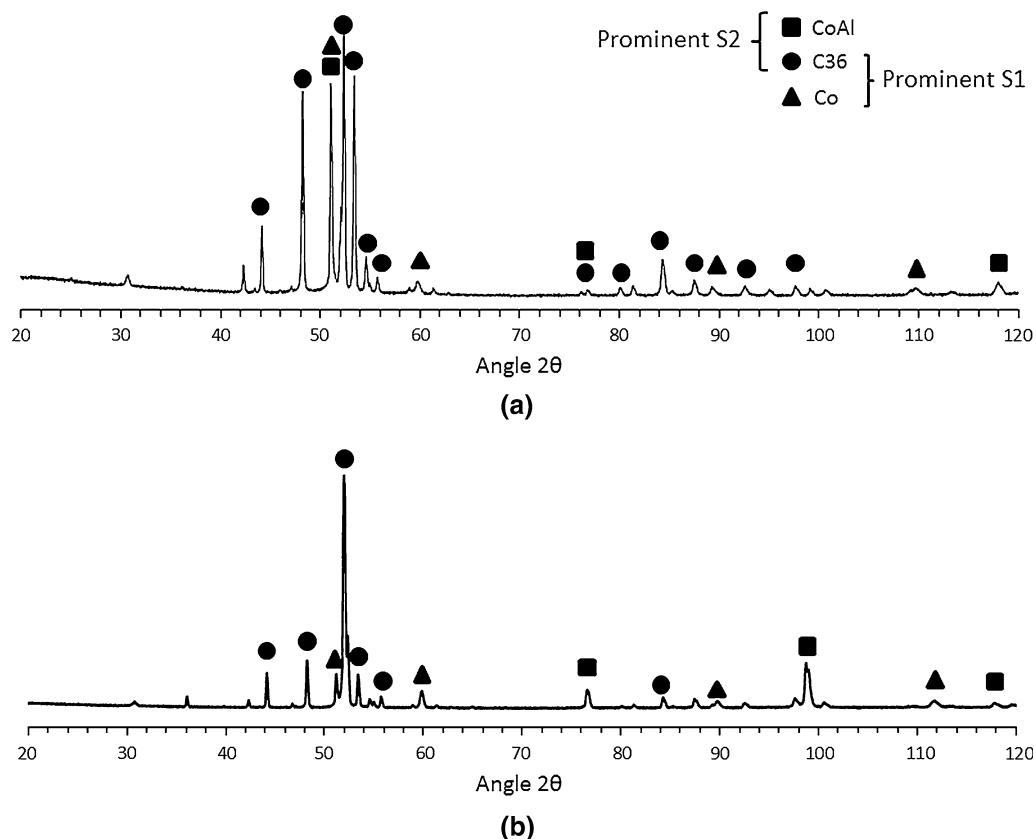
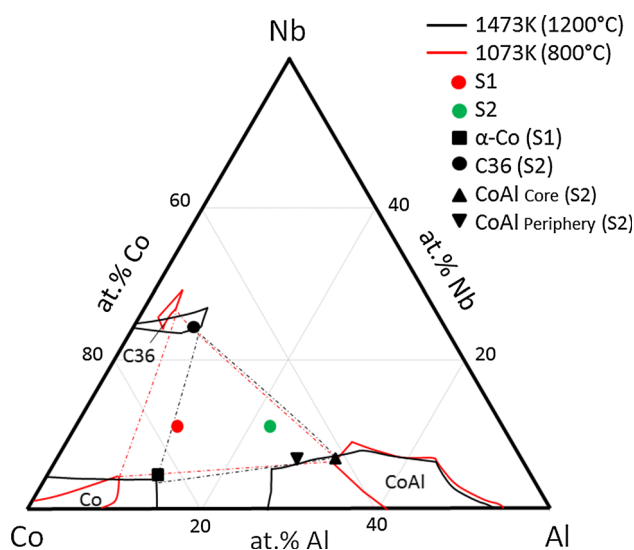Fig. 4—X-ray diffraction patterns: (a) alloy S1 and (b) alloy S2.

Fig. 5—Isothermal sections at 1473 K (1200 °C) and superimposed solute solubility at 1073 K (800 °C), showing the phase boundaries in relation to the compositions in the different phases for alloys S1 and S2. Dotted lines show tie-triangles from Ref. [15].

The extent of the ternary eutectic is limited (Figure 2(b)); therefore, terminal freezing occurs over a narrow temperature range. This is also observed in Figure 5, where the nominal composition lies very close to the α-Co—C36 tie-line at 1473 K (1200 °C). In this case, the liquid and solid compositions traverse the

metastable liquidus and solidus lines below the invariant temperature. Freezing of the terminal eutectic can occur either as L → α-Co + CoAl or L → C36 + CoAl (α-Co is the primary phase—S1) or L → CoAl + α-Co or L → C36 + α-Co (CoAl is the primary phase—S2) and depends on which phase the ternary phase (CoAl in S1 and α-Co in S2) nucleates on. From the microstructure, it is difficult to determine which of the cases is likely. It is clear, nevertheless, that the ternary eutectic cannot freeze at a single temperature, though it will freeze over a narrow temperature range, as a three-phase reaction below the invariant temperature, as mentioned previously.

B. Class II—Quasi-Peritectic Reaction

Figures 6(a) and (b) correspond to BEIs from S3 and S4, respectively. In both cases, primary freezing constitutes C14, and the average measured compositions are presented in Table III.

There is negligible microsegregation observed within the primary C14 phase. In S3, there is sporadic existence of the second phase and solidification is dominated by primary freezing. The terminal liquid is then consumed by the peritectic reaction, L + C14 → Co_2AlNb with compositions given in Table III.

On the other hand, in the case of S4 in Figure 6(b), Co_2AlNb exists as two distinct morphologies, as exemplified in Figure 6(c). The composition of the primary C14 phase and the coarse Co_2AlNb morphology were
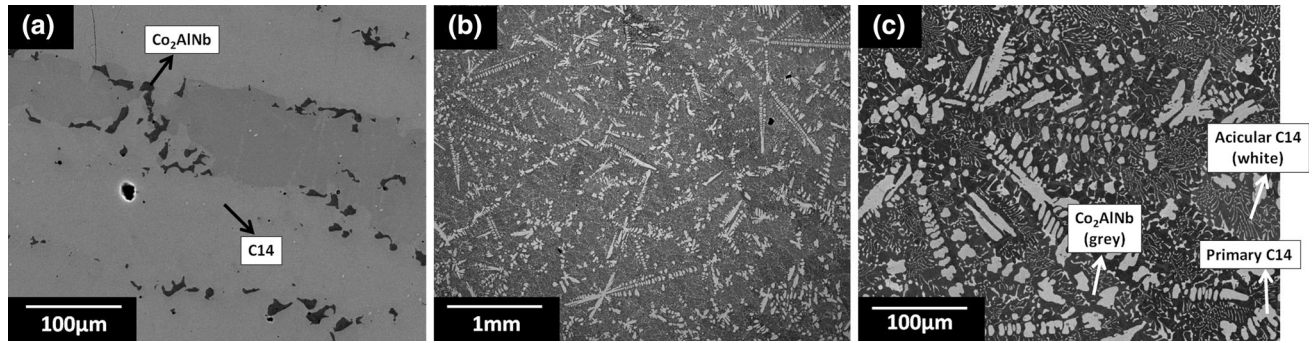
Fig. 6—(*a*) BEI for alloy S3, (*b*) low-magnification BEI for alloy S4, and (*c*) high-magnification BEI for alloy S4.

Table III. Average Composition of Phases with Standard Deviation Present in S3 and S4 (in At. Pct); Please Note that Co$_2$AlNb Composition does not Include that from the Acicular Morphology

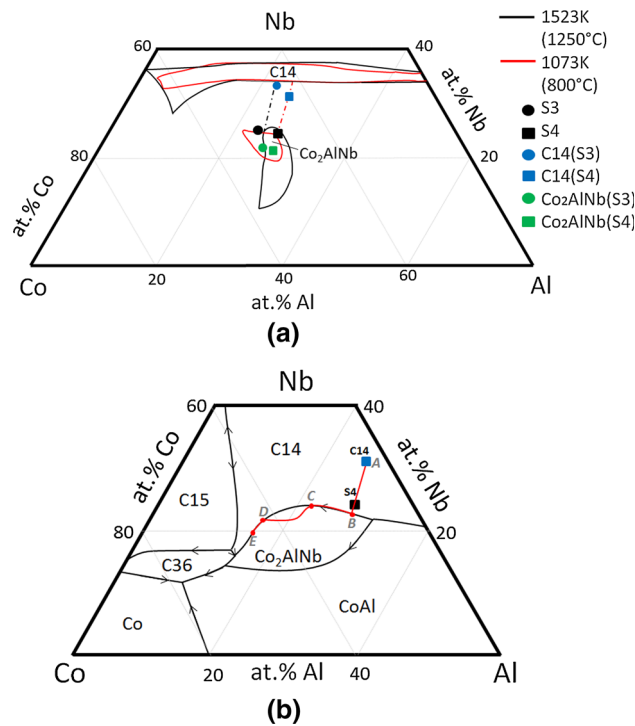| Phases	Pct Al	Pct Co	Pct Nb
C14 (S3)	22.3 ± 0.61	44.4 ± 0.92	33.3 ± 0.31
C14 (S4)	25.3 ± 0.23	43.1 ± 0.26	31.6 ± 0.06
Co$_2$AlNb (S3)	26.1 ± 0.76	51.4 ± 0.93	22.5 ± 0.43
Co$_2$AlNb (S4)	27.8 ± 0.35	51.1 ± 0.25	21.1 ± 0.45

Fig. 7—(*a*) Isothermal sections at 1523 K (1250 °C) and superimposed solute solubility at 1073 K (800 °C), showing the phase boundaries in relation to the compositions in the different phases for alloys S3 and S4. Dotted lines show tie-lines from Ref. [15]. (*b*) Liquidus projection illustrating path traversed by the liquid composition during freezing in S4.[20]

measured and are reported in Table III. The fine acicular morphology of Co$_2$AlNb precludes composition measurement owing to volume averaging effects. The tie-line joining the compositions corresponding to primary C14 and Co$_2$AlNb is presented in Figure 7(a) and refers to the isothermal sections at 1523 K and 1073 K (1250 °C and 800 °C).[15] In both cases, it is shown that the compositions in the two phases do not lie near the boundary of their respective single-phase regions at 1523 K (1250 °C), particularly for Co$_2$AlNb, indicating negligible diffusion in the solid during subsequent cooling to lower temperatures.

In the case of S3 and S4, initial primary freezing of C14 is followed by the peritectic reaction, L + C14 → Co$_2$AlNb. Since the peritectic transformation that follows the peritectic reaction never goes to conclusion, the liquid composition leaves the peritectic valley and traverses the Co$_2$AlNb liquidus surface, and in S3, freezing terminates through primary solidification of Co$_2$AlNb.[31,32] In the case of S4, a similar situation is encountered but with a difference. The peritectically formed Co$_2$AlNb phase is labeled "grey" in Figure 6(c), as in the case of S3. However, if all of the liquid has not been consumed during primary freezing of Co$_2$AlNb (governed by back diffusion in the solid), the liquid composition will reintersect the C14-Co$_2$AlNb valley. However, the C14-Co$_2$AlNb valley in the liquidus projection changes from peritectic to eutectic with decreasing temperature; *i.e.*, for Al <20 at. pct and Nb <20 at. pct, the valley is eutectic in nature.[20] Consequently, the reintersection of the liquid composition with the C14-Co$_2$AlNb valley results in the eutectic reaction, L → C14 + Co$_2$AlNb. The path traversed by the liquid composition during freezing of S4 is schematically illustrated in the liquidus projection in Figure 7(b). Here, AB refers to primary freezing of C14, BC corresponds to the peritectic reaction and incomplete peritectic transformation, CD refers to primary freezing of Co$_2$AlNb, and DE represents the terminal eutectic reaction, when all liquid is consumed
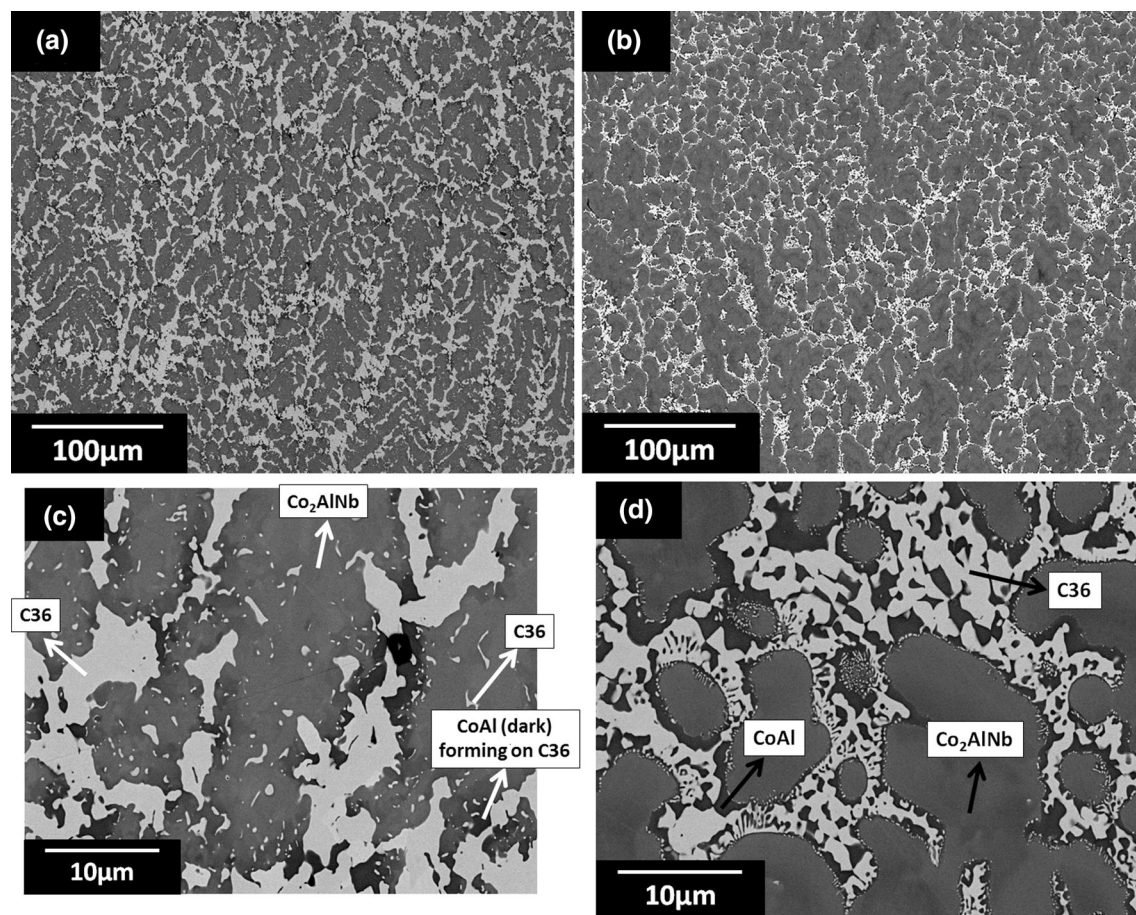
Fig. 8—(*a*) Low-magnification BEI for alloy S5, (*b*) low-magnification BEI for alloy S6, (*c*) high-magnification BEI for alloy S5, and (*d*) high-magnification BEI for alloy S6.

Table IV. Average Composition of Phases with Standard Deviation Present in S5 and S6 (in At. Pct)

Phases	Pct Al	Pct Co	Pct Nb
Co$_2$AlNb (S5)	27.4 ± 0.10	52.5 ± 0.13	20.1 ± 0.17
Co$_2$AlNb (S6)	30.8 ± 0.36	54.3 ± 0.10	14.9 ± 0.36
C36 (S5)	9.9 ± 0.44	64.3 ± 0.62	25.8 ± 0.22
C36 (S6)	6.9 ± 0.21	69.3 ± 0.24	23.8 ± 0.41
CoAl (S5)	27.9 ± 1.38	64.0 ± 2.48	8.2 ± 1.10
CoAl (S6)	27.7 ± 0.75	65.0 ± 1.65	7.4 ± 0.94

at E. Since the peritectically formed Co$_2$AlNb isolated the prior C14 primary phase from the liquid, the eutectic reaction requires nucleation of C14, but this will occur on Co$_2$AlNb. It is this "renucleated" C14 phase growing as the (C14 + Co$_2$AlNb) eutectic that exhibits the acicular-type morphology. In fact, a similar phenomenon was also observed in the Fe-Al-Nb ternary system, where, following primary freezing of Nb followed by the peritectic reaction, L + Nb → Nb$_2$Al, the class II reaction, L + Nb$_2$Al → Nb + μ, requires nucleation of both these phases on Nb$_2$Al.[34]

Figures 8(a) and (b) present the microstructure corresponding to S5 and S6, where Co$_2$AlNb, C36, and CoAl are the expected phases in the as-cast microstructure. In both cases, the primary phase to freeze is

Co$_2$AlNb. The measured compositions in the primary phase are presented in Table IV. Figures 8(c) and (d) show the microstructures of S5 and S6, respectively, in more detail. For both alloys, there is also the existence of C36 (bright) and CoAl (dark), and the measured compositions in these phases are given in Table IV.

The compositions are included in the isothermal sections at 1523 K (1250 °C) and 1073 K (800 °C), in Figure 9(a), corresponding to the phases found in S5 and S6 and their nominal compositions. For S6, particularly, there is reasonable agreement between the measured composition of C36 (4 at. pct higher Co) with respect to the corresponding vertex of the tie-triangle at 1523 K (1250 °C). However, significant deviation exists in the case of CoAl and Co$_2$AlNb. The line joining the
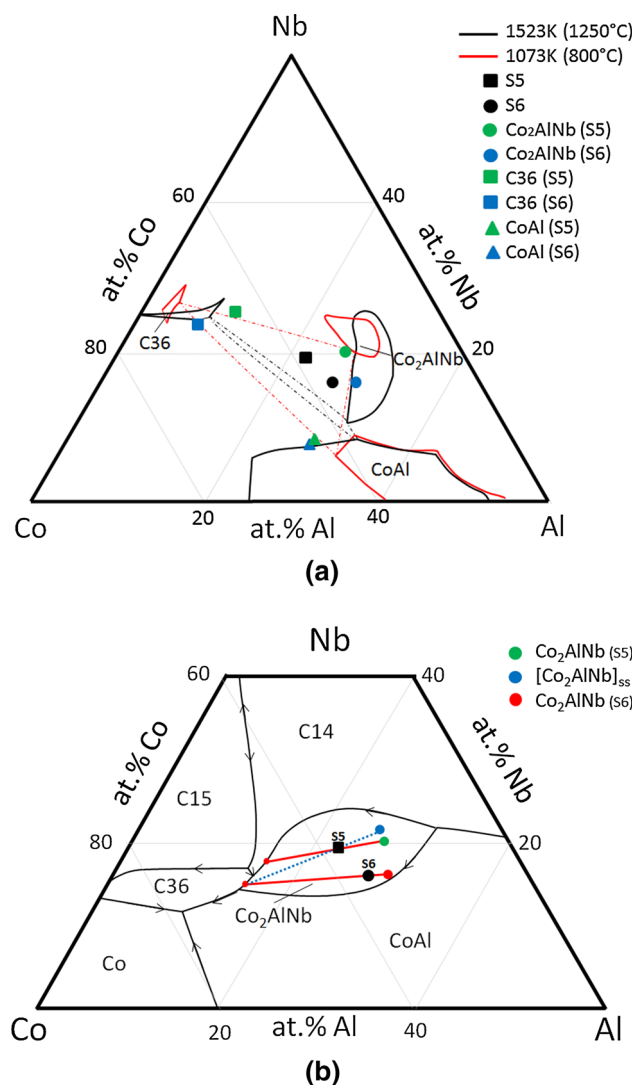
Fig. 9—(a) Isothermal sections at 1523 K (1250 °C) and superimposed solute solubility at 1073 K (800 °C), showing the phase boundaries in relation to the compositions in the different phases for alloys S5 and S6. Dotted lines are tie-triangles from Ref. [15]. (b) Liquidus projection illustrating path traversed by the liquid composition during freezing in S5 and S6.[20]

measured compositions are also plotted in Figure 9(a). From the isothermal section at 1523 K (1250 °C), the Class II reaction is not expected to occur, since the nominal composition falls markedly outside the tie-triangle. The composition of Co_2AlNb lies on the boundary of the single-phase region, and there is distinct supersaturation of Al in C36 at 1523 K (1250 °C) and more so at 1073 K (800 °C).

From the liquidus projection in Figure 9(b), following primary freezing of Co_2AlNb, L → Co_2AlNb, the eutectic reaction, L → Co_2AlNb + C36, occurs with a divorced morphology, as observed in Figure 8(c). Therefore, following primary freezing, the liquid composition traverses the Co_2AlNb liquidus surface and must then intersect the Co_2AlNb-C36 valley. This is given by the intersection of the line joining the measured Co_2AlNb and nominal composition corresponding to S5 with the Co_2AlNb-C36 eutectic valley. However, this is not observed in Figure 9(b) as expected, owing to the solid-state precipitation of C36 in Co_2AlNb. Solid-state precipitation of C36 in Co_2AlNb implies that Co_2AlNb is supersaturated in primarily Co and Nb (C36 is concentrated in Co and Nb), which is observed in the isothermal section at 1073 K (800 °C) in Figure 9(a). The solid-state precipitation of C36, therefore, can be represented as $[Co_2AlNb]_{ss}$ → Co_2AlNb + C36. The microstructure within the dendrites is a mixture of Co_2AlNb + C36, and the measured composition of the primary phase corresponds to Co_2AlNb and not $[Co_2AlNb]_{ss}$. In fact, the straight line joining the composition corresponding to $[Co_2AlNb]_{ss}$ and nominal composition of S5 would have intersected the Co_2AlNb-C36 eutectic valley, as schematically shown in Figure 9(b). Additionally, CoAl is also present in the microstructure. From the isothermal section at 1073 K (800 °C), it is clear that C36 is supersaturated in Al, therefore resulting in the solid precipitation of CoAl occurring *via* $[C36]_{ss}$ → C36 + CoAl. The solid-state precipitation of CoAl within C36 and C36 within Co_2AlNb clearly accounts for the difference between the microstructures in S5 and S6, where, in the latter, CoAl forms as a divorced eutectic with C36 through a eutectic reaction.

measured Co_2AlNb composition and the nominal composition corresponding to S6 intersects the Co_2AlNb-C36 eutectic valley, as observed in the liquidus projection in Figure 9(b). Therefore, primary freezing, L → Co_2AlNb, will be followed by the eutectic reaction, L → Co_2AlNb + C36. Beyond the invariant temperature, as the liquid is not consumed, CoAl has to nucleate, and it can be observed that CoAl nucleates on the Co_2AlNb dendrite lobes in Figure 8(d). Further growth of the (C36 + CoAl) eutectic then occurs with a divorced morphology corresponding to L → C36 + CoAl.

However, in the case of S5, a distinctly different microstructure is observed. There is evidence of solid-state precipitation of C36 within the primary Co_2AlNb phase, and consequently, the (C36 + CoAl) morphology is markedly different from that observed in S6. The

IV. CONCLUSIONS

The freezing sequence in the Nb-Al-Co ternary system in the Co-rich corner with emphasis on the Laves and Heusler phases was examined. The following conclusions can be drawn:

1. In the case of the (α-Co + CoAl + C36) ternary eutectic, the measured compositions for α-Co and C36 phases show good agreement with the corresponding vertices of the tie-triangle in the 1473 K (1200 °C) isothermal section. Negligible solute solubility occurs during cooling, and the measured phase compositions of α-Co and C36 can be taken as the corresponding vertices for the tie-triangle.

2. Care must be taken in the interpretation of the microstructure, because there is a narrow composi-

tion window that permits the Class II reaction. When not all liquid has been consumed, the liquid composition reintersects the (C14-Co_2AlNb) valley and forms a new and finer eutectic. The measured composition of C36 is in good agreement with the corresponding vertex of the tie-triangle in the 1523 K (1250 °C) isothermal section.

3. When the quasi-peritectic reaction does not occur, depending on the initial composition, solid-state precipitation of C36 and CoAl does occur within supersaturated Co_2AlNb and C36 phases, respectively. The resultant microstructure in this instance is markedly different from the quasi-peritectic case.

REFERENCES

1. R.C. Reed: *The Superalloys: Fundamentals and Applications*, Cambridge University Press, Cambridge, 2006.
2. H.J. Dai, J.C. Gebelin, M. Newell, R.C. Reed, N. D'Souza, P.D. Brown, and H.B. Dong: *Superalloys 2008*, TMS, Warrendale, PA, 2008, pp. 367–74.
3. L.S. Luo, Y.Q. Su, J.J. Guo, X.Z. Li, S.M. Li, H. Zhong, L. Liu, and H.Z. Fu: *J. Alloys Compd.*, 2008, vol. 461, pp. 121–27.
4. G. Ghosh and G.B. Olson: *Acta Mater.*, 2007, vol. 55, pp. 3281–3303.
5. L. Zhu, C. Wei, H. Qi, L. Jiang, Z. Jin, and J.C. Zhao: *J. Alloys Compd.*, 2017, vol. 691, pp. 110–18.
6. J.R. Davis: *ASM Specialty Handbook: Nickel, Cobalt, and their Alloys*, ASM International, Materials Park, OH, 2000.
7. N. D'Souza, M. Lekstrom, and H.B. Dong: *Mater. Sci. Eng. A*, 2008, vol. 490, pp. 258–65.
8. L. Machon and G. Sauthoff: *Intermetallics*, 1996, vol. 4, pp. 469–81.
9. G. Sauthoff: *Intermetallics*, 2008, vol. 8 (1), pp. 1101–09.
10. G. Sauthoff: *Intermetallics*, VCH, Weinheim, 1995.
11. B. Zeumer and G. Sauthoff: *Intermetallics*, 1997, vol. 5, p. 563.
12. P. Hanus, P. Batrsch, M. Palm, R. Krein, K. Bauer-Partenheimer, and P. Janschek: *Intermetallics*, 2010, vol. 18, pp. 1379–84.
13. D.D. Risanti and G. Sauthoff: *Intermetallics*, 2011, vol. 19, pp. 1727–36.
14. M. Takeyama and C.T. Liu: *Mater. Sci. Eng. A*, 1991, vol. 132, p. 61.
15. O. Dovbenko, F. Stein, M. Palm, and O. Prymak: *Intermetallics*, 2010, vol. 18, pp. 2191–2207.
16. V.Y. Markiv, Y.V. Voroshilov, P.I. Kripyakevich, and E.E. Cherkashin: *Sov. Phys. Crystallogr.*, 1965, vol. 9, pp. 619–20.
17. K.H.J. Buschow, P.G. van Engen, and R.J. Jongebreur: *Magn. Mater.*, 1983, vol. 38, pp. 1–22.
18. K.C. Hari Kumar, I. Ansara, P. Wollants, and L. Dalaey: *J. Alloys Compd.*, 1998, vol. 267, pp. 105–12.
19. F. Stein, D. Jiang, M. Pal, G. Sauthoff, and D. Grunner: *Intermetallics*, 2008, vol. 16 (6), pp. 785–92.
20. M. Palm, C. He, O. Dovbenko, F. Stein, and J.C. Schuster: *J. Phase Equilib. Diff.*, 2012, vol. 3, pp. 210–21.
21. W. Kurz and D.J. Fisher: *Fundamentals of Solidification,* Trans Tech Publications, Zurich, 1986, vol. 1, pp. 134–36 and 221–24.
22. H.B. Dong and R. Brooks: *Mater. Sci. Eng. A*, 2005, vol. 413, pp. 480–84.
23. H.D. Brody and M.C. Flemings: *Trans. Met. Soc. AIME*, 1966, vol. 236, pp. 615–24.
24. C.A. Nunes, R. Sakidja, Z. Dong, and J.H. Perpezko: *Intermetallics*, 2000, vol. 8, pp. 327–37.
25. D.R.F. West and N. Saunders: *Ternary Phase Diagrams in Materials Science,* 3rd ed., Institute of Metals, 2002, pp. 49–52.
26. H.B. Dong, M.R.M. Shin, E.C. Kurum, H. Cama, and J.D. Hunt: *Fluid Phase Equilib.*, 2003, vol. 212, pp. 199–208.
27. V.T. Witusiewicz, A.A. Bondar, U. Hecht, V.M. Voblikov, N.I. Tsyganenko, O.S. Fomichov, M.V. Karpets, V.M. Petyukh, and T.Y. Velikanova: *J. Mater. Sci.*, 2013, vol. 48, pp. 377–412.
28. E.C. Kurum, H.B. Dong, and J.D. Hunt: *Metall. Mater. Trans. A*, 2005, vol. 36A, pp. 3103–10.
29. N. D'Souza, L.M. Feitosa, G.D. West, N.G. Jones, and H.B. Dong: *J. Alloys Compd.*, 2017, vol. 698, pp. 375–83.
30. W Wei Li, D Fu Ping, and W Bing Bo: *Sci. China Ser. G Phys. Mech. Astron.*, 2007, vol. 50, pp. 472–90.
31. M. Hillert: *Solidification and Casting of Metals*, The Metals Society, London, 1979, pp. 81–87.
32. H.W. Kerr and W.K.: *Int. Mater. Rev.*, 1996, vol. 41 (4), pp. 129–64.
33. N. D'Souza, R. Beanland, C. Hayward, and H.B. Dong: *Acta Mater.*, 2011, vol. 59, pp. 1003–13.
34. F. Stein, C. He, O. Prymak, S. Voß, and I. Wosack: *Intermetallics*, 2015, vol. 59, pp. 43–58.